International Journal of Biological Macromolecules xxx (2014) xxx–xxx

Contents lists available at ScienceDirect

International Journal of Biological Macromolecules

journal homepage: www.elsevier.com/locate/ijbiomac

Fabrication of a novel naltrexone biosensor based on a computationally engineered nanobiocomposite

Q1 Mohammad-Bagher Gholivand[a,*], Ali R. Jalalvand[a,b], Giti Paimard[a], Hector C. Goicoechea[b], Thomas Skov[c], Reza Farhadi[a], Sirous Ghobadi[d], Nozar Moradi[a], Vahid Nasirian[a]

[a] Faculty of Chemistry, Razi University, Kermanshah 671496734, Iran
[b] Laboratorio de Desarrollo Analítico y Quimiometría (LADAQ), Cátedra de Química Analítica I, Universidad Nacional del Litoral, Ciudad Universitaria, CC 242, S3000ZAA Santa Fe, Argentina
[c] Quality & Technology, Department of Food Science, Faculty of Science, University of Copenhagen, Copenhagen, Denmark
[d] Department of Biology, Faculty of Science, Razi University, Kermanshah, Iran

ARTICLE INFO

Article history:
Received 7 March 2014
Received in revised form 8 July 2014
Accepted 9 July 2014
Available online xxx

Keywords:
Biosensor
Naltrexone
Bovine serum albumin
Fullerene-C_{60}
Computational and experimental characterizations

ABSTRACT

A computationally engineered impedimetric naltrexone (NLT) biosensor based on immobilization of bovine serum albumin (BSA) onto fullerene-C_{60}/glassy carbon electrode (FLR/GCE) has been developed using initial characterization by computational methods and complementing them by experimental ones. Computational results showed that BSA hydrophobically binds to FLR which is energetically favorable and leads to the spontaneous formation of the stable nanobiocomposite and also showed that interaction of NLT with BSA is mainly driven by hydrogen bonding and hydrophobic interactions. Besides complementing the computational studies, experimental results showed that addition of FLR to the surface of the electrode facilitated electron transfer reactions, and also showed that the presence of BSA inhibits the interfacial electron transfer in some extent due to the non-conductive properties of BSA. The presence of NLT may form a negatively charged electroactive complex with BSA which repels the negatively charged redox probe and decelerates interfacial electron transfer leading to obvious faradaic impedance change. The faradaic impedance responses were linearly related to naltrexone concentration between 0.1 nM and 80 nM and limit of detection (LOD) was calculated to be 0.01 nM $3S_b/b$. Finally, the proposed biosensor was successfully applied to determination of NLT in urine samples of both healthy and addict volunteers.

1. Introduction

Naltrexone hydrochloride (NLT, Fig. 1A), was synthesized in 1965 and is a potent opioid antagonist which reversibly blocks opioid receptors and has been approved by the FDA for treating both alcohol and opioid dependence [1]. The blockade of opioid receptors is its mechanism in the management of opioid dependence. The mechanism of action in alcohol dependence may be due to the modulation of the dopaminergic mesolimbic which ethanol is believed to activate [2]. Due to clinical importance of NLT, it has been measured by different analytical techniques including: thin layer chromatography (TLC) [3], gas chromatographic (GC) methods [4–13], high-performance liquid chromatography (HPLC) with UV or electrochemical detection [14–24], liquid chromatography–mass spectroscopy (LC–MS) [25], LC–electrospray ionization tandem mass spectrometry [26,27], chemiluminescence [28], flow-injection analysis with amperometric detection [29], spectrofluorimetry [30], and voltammetry [31]. Electrochemical techniques can be considered as a powerful technique for the determination of pharmaceutical compounds in biological fluids [32,33]. Among electrochemical methods, electrochemical impedance spectroscopy (EIS), becomes increasingly

Abbreviations: BSA, bovine serum albumin; HSA, human serum albumin; NLT, naltrexone hydrochloride; FLR, fullerene-C60; GCE, glassy carbon electrode; SEM, scanning electron microscopy; EIS, electrochemical impedance spectroscopy; CV, cyclic voltammetry; EIS, electrochemical impedance spectroscopy; LOD, limit of detection; UPW, ultrapure water; SCE, saturated calomel electrode; MVD, Molegro Virtual Docker; TBS, Tris buffer solution; RSD, relative standard deviation; TLC, thin layer chromatography; GC, gas chromatography; HPLC, high-performance liquid chromatography; LC–MS, liquid chromatography–mass spectroscopy.

* Corresponding author. Tel.: +98 831 4274557; fax: +98 831 4274559.
E-mail addresses: mbgholivand2013@gmail.com, mbgholivand@yahoo.com (M.-B. Gholivand).

http://dx.doi.org/10.1016/j.ijbiomac.2014.07.028
0141-8130/

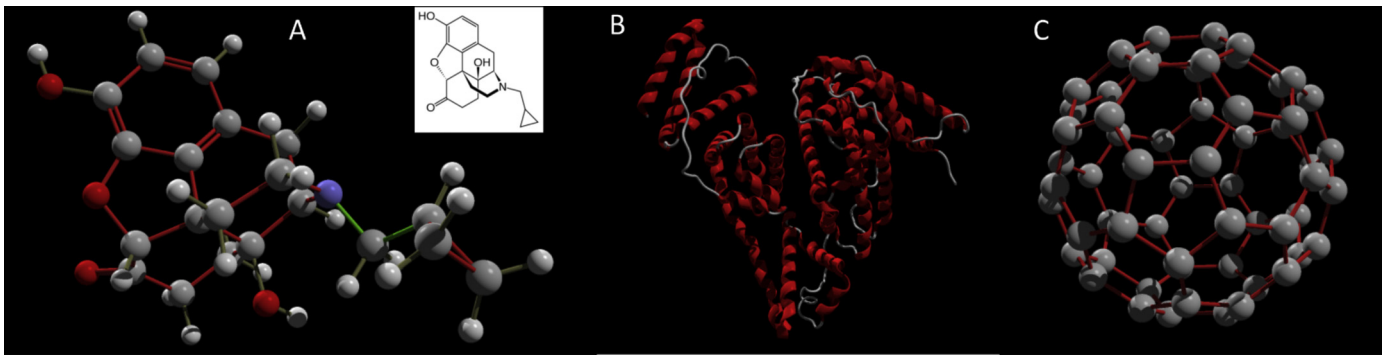

Fig. 1. (A) Molecular structure of NLT represented by ball and stick model, (B) three-dimensional structure of BSA (chain A) represented by solid ribbon, and (C) structure of the FLR designed by Nanotube Modeler software represented by ball and stick model.

popular because it offers several advantages such as simplicity, high sensitivity and serving as an elegant way to interface biorecognition events and signal transduction.

Among biomacromolecules, serum albumin is a soluble protein which commonly serves as a depository and a transport molecule for many exogenous compounds. Bovine serum albumin (BSA, Fig. 1B) is one of the most extensively studied of this group of proteins, particularly because of its structural homology with human serum albumin (HSA). The direct electron transfer between proteins and the electrode surface has received considerable attention, because it can be used in fabricating new generation of biosensor devices. Since redox centers are deeply buried within the proteins molecules, the electron transfer between proteins and the electrode is difficult. Therefore, different substrates could be used to immobilize proteins on the electrode surfaces. Fullerenes have been widely studied attributing to their unique structural, electronic and spectroscopic properties since their discovery by Kroto et al. [34,35]. They have also been exploited for diverse applications in the fields of biology, chemistry and nanoscience [36,37]. As every carbon in a fullerene C_{60} (FLR, Fig. 1C) is a surface atom, the electron transport of this material is highly sensitive to the surface-adsorbed molecules [38]. Especially, as an electron acceptor, FLR displays rich electrochemistry because of its unique dimensional and electronic structures [39]. Recently, the electrochemical behavior of FLR films in aqueous solutions has been investigated [40]. The most promising result of these studies is that the partially reduced FLR films are sufficiently conductive to be used for modified electrodes, leading to favorable electrocatalytic properties [41–44].

The objective of this study is to develop a novel, ultrasensitive, selective and simple impedimetric NLT biosensor with good stability, reproducibility and repeatability for the determination of NLT using unique properties of BSA/FLR nanobiocomposite which can be directly applied in urine samples without expensive and time-consuming pretreatments. To demonstrate the general design of the BSA/FLR nanostructure based biosensing platform, we first used computational studies for a proof of concept and then completed them by experimental observations. This valuable study describes results obtained by a combination of computational and experimental techniques to develop an ultrasensitive BSA/FLR/GCE biosensor to direct determination of NLT in urine samples in both healthy and addict subjects. To the best of our knowledge, this work is the first report on the impedimetric NLT biosensor.

2. Experimental

2.1. Chemicals and solutions

The BSA (M = 66,487, free of fatty acids with an electrophoresis grade), NLT, and FLR (purity 99.9%) were purchased from Sigma Aldrich (St. Louis, MO, USA). All other reagents employed were of analytical grade and received from Merck. A concentration of 0.05 M Tris buffer solution (TBS) was used to control the pH at 7.40. $[Fe(CN)_6]^{3-/4-}$ solution (redox probe, 5.0 mM) was prepared in TBS (0.05 M, pH 7.4) and used for the measurements. All solutions were prepared by ultrapure water (UPW).

2.2. Instrumentation and softwares

Electrochemical experiments were performed using a μ-AutolabIII/FRA2 driven by the Nova 1.8 software. A conventional three-electrode cell was used with a saturated calomel electrode (SCE) as reference electrode, a Pt wire as counter electrode and a bare or modified GCE as working electrode. The SEM experiment was made on a KYKY-EM 3200 scanning electron microscope. All fluorescence spectra were measured on a Cary Eclipse fluorescence spectrophotometer equipped with a water bath and a 1.0 cm quartz cell. The UV–vis spectra were measured on an Agilent 8453 UV–vis controlled by the Agilent UV–vis ChemStation software. A JENWAY-3345 pH-meter equipped with a combined glass electrode was used to pH measurements. HPLC analyzes reported in this study were carried out by a Medical Diagnostic Laboratory in Kermanshah, Iran whose instrument was an 1100 Series HPLC from Agilent Technologies equipped with a binary pump, degasser, an auto sampler, a solvent tray and multiple wavelength detector. The statistical analysis of the sequence of BSA (chain A) was performed using CLC Main Workbench software (version 6.0). The three-dimensional structure of FLR was generated using Nanotube Modeler software (Fig. 1C). The FLR was then docked to the BSA using Molegro Virtual Docker (MVD) software. The chemical structure of the NLT was constructed by Hyperchem package (version 8.0), and energy minimization for NLT was performed by AM1 semi empirical method with Polak–Ribiere algorithm until the root mean square gradient of 0.01 kcal mol^{-1}. The MVD software was also employed to generate a docked conformation of NLT with BSA. LIGPLOT [45], a program for automatically plotting protein-ligand interactions, was used for analyzing the interactions between NLT and BSA. The recorded experimental data was smoothed, when necessary, and converted to matrices by means of several homemade MATLAB (version 7.14) m-files. All computations were performed on a DELL XPS laptop (L502X) with Intel Core i7-2630QM 2.0 GHz, 8 GB of RAM and Windows 7-64 as its operating system.

2.3. Preparation of the electrochemical biosensor

The bare GCE was polished with alumina powder and then zinc oxide before modifications. It was then washed with 20.0 mL phosphoric acid solution (0.1 M) to remove the adhered powder,

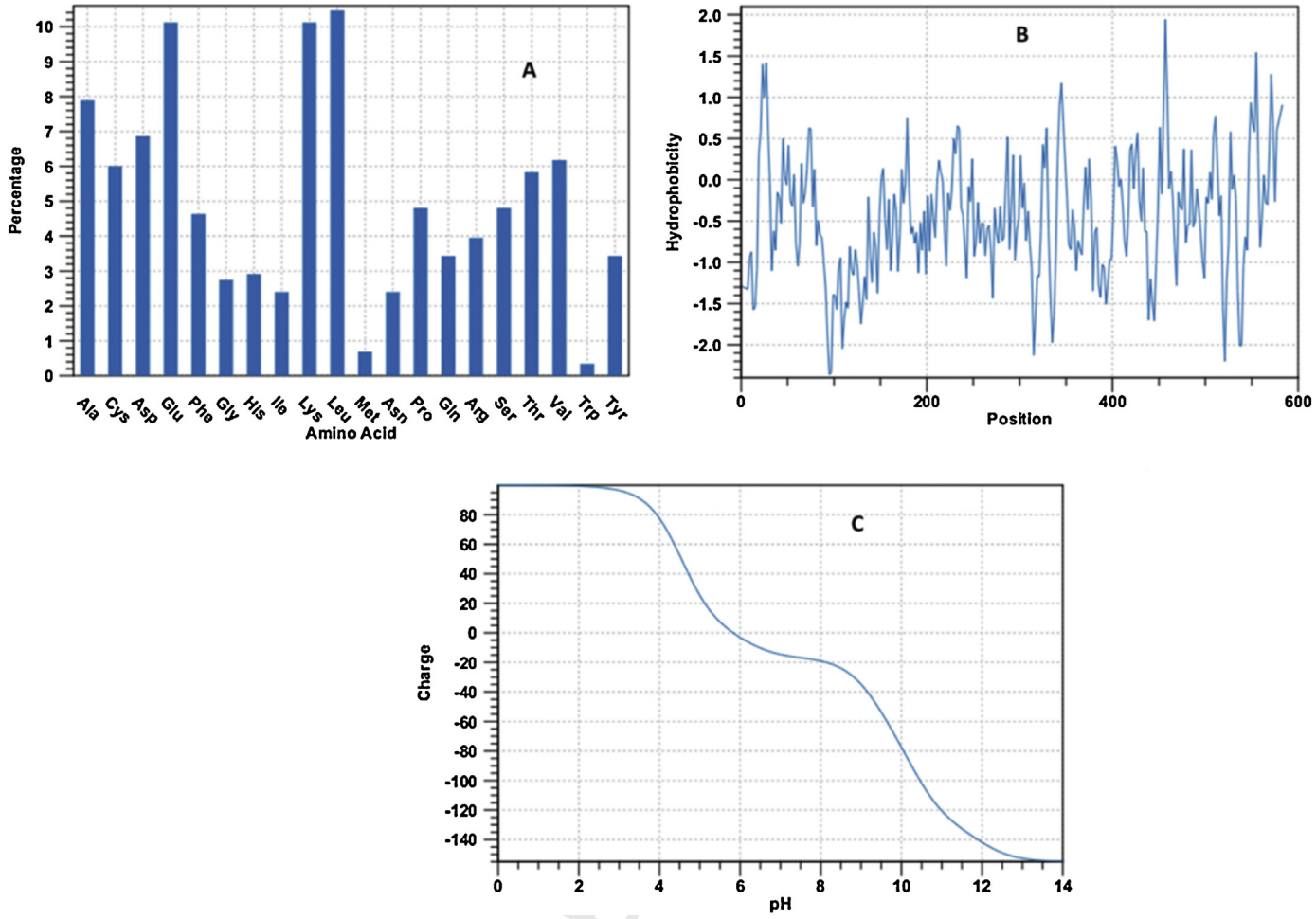

Fig. 2. Results of protein analysis: (A) amino acid distribution histogram, (B) hydrophobicity plot, and (C) electrical charge as a function of pH.

and rinsed with UPW after which the electrode was dried. A stock solution of FLR (0.65 mg mL^{-1}) was prepared by dissolving an appropriate amount of its solid powder in dichloromethane. A known volume (20.0 μL) of this solution was casted onto the surface of the clean and dried GCE using a micropipette and dried in a stream of warm air (40.0 °C). The FLR/GCE surface was then pretreated by partially reducing the FLR film in 1.0 M potassium hydroxide in the potential range 0.0 to −1.5 V with a 10.0 mV s^{-1} scan rate according to the procedure described by Szucs et al. [46]. On partially reducing a FLR film, it becomes conducting and hence can be used as a modifier having special electrocatalytic properties. Subsequently, the electrode is placed in the TBS (0.05 M, pH 7.4), which was previously de-oxygenated with high purity nitrogen for 15.0 min. The FLR/GCE was then ready for use.

The BSA/FLR/GCE was prepared with the following procedure: an 8.0 μL of the BSA (0.2 mg mL^{-1} dissolved in TBS, 0.05 M, pH 7.4) was dripped on the FLR/GCE surface and dried at room temperature to form a stable gel-like film. In some cases the fabricated BSA/FLR/GCE was transferred to a NLT solution (10.0 nM) and incubated for 15.0 min. Then, the electrode was extensively rinsed and subjected to electrochemical measurements. To refresh the bare GCE surface it was sonicated in 0.1 M hydrochloric acid for 10.0 min and then acetonitrile for 10.0 min. The electrode surface was dried and then sensed again with the same composition for further experiments.

2.4. Preparation of the real samples

A blank human serum sample (drug-free) was provided by a healthy volunteer, not exposed to any drug for at least 10.0 months. An actual human serum sample was collected from a person who was addicted to opium. According to the method of Han et al. [47], to eliminate protein and other substances, 1.0 mL of human serum sample was placed in a 10.0 mL glass tube and 1.0 mL of 15% (w/v) zinc sulfate solution-acetonitrile (50/40, v/v) was added. The glass tube was vortexed for 20.0 min, maintained at 4.0 °C for 15.0 min followed by centrifugation at 4000.0 rpm for 5.0 min. Then, the supernatant was collected in the same tube and this solution was diluted to 5.0 mL using UPW.

3. Results and discussion

3.1. Computational studies

In order to obtain suitable information related to the interaction of BSA with FLR, the sequence and the crystal structure of BSA (chain A) were theoretically analyzed. The statistical results showed the selected chain of the BSA contains 583.0 amino acids (Fig. 2A), approximately 40.1% were hydrophobic (A, F, G, I, L, M, P, V, and W) and 25.9% were hydrophilic (C, N, Q, S, T, and Y) residues, Fig. 2B. Furthermore, the computational results confirmed that the BSA has approximately the same number of negative and positive groups on

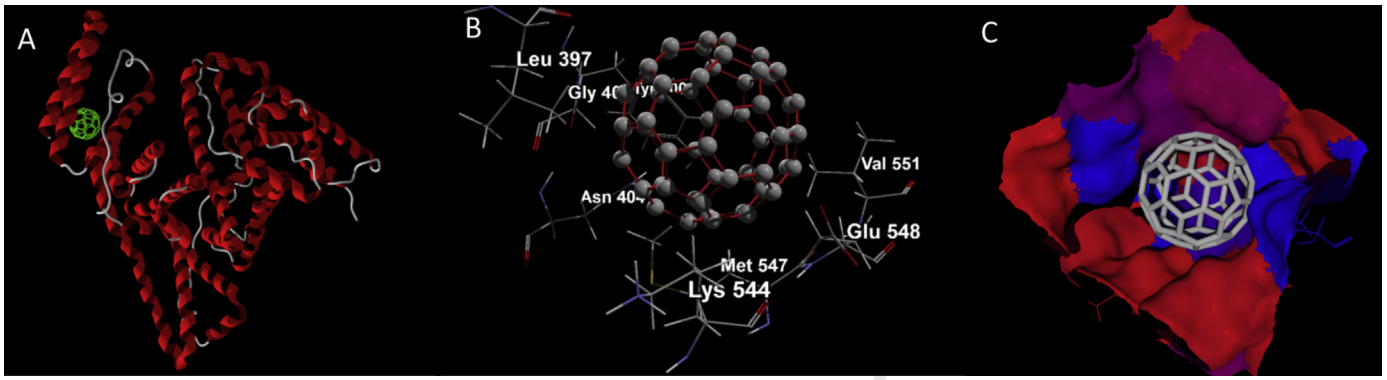

Fig. 3. Computational interaction models of BSA–FLR: (A) BSA represented by solid ribbon and FLR is represented by stick, and (B) the residues of BSA are represented by sticks (thin) and the FLR is represented by ball and stick model, and (C) hydrophobicity view: binding pockets of protein are represented by hydrophobic interaction and FLR is represented using stick model.

its surface, and the calculated isoelectric point was approximately 5.2, Fig. 2C. According to these results, it is reasonable to expect that the interaction of the BSA with FLR will be driven by a combination of hydrophobic and hydrophilic interactions, where the anterior prevails over the latter.

Subsequently, molecular docking studies were performed to identify the potential interaction sites, assuming that the FLR (considered as ligand) would freely rotate around the entire structure of the BSA. Such docking studies allowed us to identify the most likely manner by which FLR was bound to BSA. The docking results with three different views are shown in Fig. 3A–C. An additional advantage of the docking studies is the possibility to identify the residues of BSA that interact with FLR. As can be seen, FLR is surrounded by Leu 397, Gly 401, Tyr 400, Asn 404, Val 551, Glu 548, Met 547, and Lys 544. The interaction of BSA with FLR seems to be dominated by hydrophobic interactions. The binding constant (K_a) and free energy change (ΔG) for the binding of FLR to BSA were $3.8 \times 10^4\ M^{-1}$ and $-14.35\ kJ\ M^{-1}$, respectively. Therefore, it is also reasonable to expect that the interaction of BSA with FLR will be energetically favorable, leading to the spontaneous formation of the nanobiocomposite. Therefore, such interaction supports the possibility of using a BSA/FLR nanobiocomposite for analytical purposes.

The MVD software was also used to realize the binding mode of NLT at the BSA. The dockings results with three different views are shown in Fig. 4A–C. As can be seen, NLT is surrounded by Ala 349, Ala 212, Leu 346, Ser 343, Arg 347, Val 481, Leu 480, Ser 201, Ser 479, Phe 205, Lys 350, Ser 201, and Arg 208. The K_a and ΔG for the binding of NLT to BSA were calculated to be $2.8 \times 10^5\ M^{-1}$ and $-17.71\ kJ\ M^{-1}$, respectively. LIGPLOT was used to explore the mode of interaction of NLT with BSA as shown in Fig. 4D. One hydrogen bonding interaction is observed between the hydroxyl group of NLT and Arg 208 of BSA, with a distance of 2.94 Å. Based on this information, it is reasonable to expect that the interaction of the NLT with BSA is mainly driven by hydrogen bonding and hydrophobic interactions.

3.2. Experimental studies

3.2.1. Summarized fluorescence quenching and UV–vis absorption studies

3.2.1.1. Fluorescence quenching studies. In order to examine the results of computational studies, the interaction of FLR with BSA was also monitored with fluorescence spectroscopy by recording the fluorescence spectra in the TBS (0.05 M, pH 7.4) at three different temperatures including 298.15, 304.15, and 310.15 K, and the representative spectra at 298.15 are shown in Fig. 5A. A gradual increase in FLR concentration in the solutions of BSA caused a decrease in fluorescence intensity without notable changes in the maximum emission wavelength (λ_{max}). In order to further analyze the studied system, the well-known Stern–Volmer equation (Eq. (1)) was used to analyze the quenching data.

$$\frac{F_0}{F} = 1 + k_q \tau_0 [Q] = 1 + K_{SV}[Q] \quad (1)$$

where F_0 and F represent the fluorescence intensities in the absence and in the presence of quencher (FLR), k_q is the quenching rate constant of the biomolecule, K_{SV} is the dynamic quenching constant, τ_0 is the average lifetime of the molecule, 10^{-8}, and [Q] is the concentration of the FLR [48]. Variations of F_0/F versus [Q] were plotted at 298.15, 304.15, and 310.15 K (not shown), and by linear regression of the plots, the K_{SV} values were calculated to be 0.0431, 0.0383, 0.0311 M^{-1}, respectively, decreasing with temperature. Therefore, we concluded that the studied quenching process is a static quenching.

Results of fluorescence spectroscopic measurements can be used to estimate the binding constant of the BSA–FLR hybrid complex by a different form of the Stern–Volmer equation [49]:

$$\log\left(\frac{F_0 - F}{F}\right) = \log\ K_a + n \log[Q] \quad (2)$$

where F_0, F, and [Q] are the same as in Eq. (1), n is the number of binding sites, and K_a is the binding constant. A plot of $\log[(F_0 - F)/F]$ versus $\log[Q]$ yields $\log K_a$ as the intercept and n as the slope. The K_a and n values obtained at 298.15, 304.15, and 310.15 K are given in Table 1. Values of n were approximately equal to 1.0, which indicated that the existence of one binding sites in BSA for FLR. The estimated values of K_a indicated that there is a moderately strong interaction between FLR and BSA.

The interaction forces between ligands and proteins include hydrogen bonds, van der Waals forces, electrostatic forces, and hydrophobic interaction forces [48]. According to Ross' view [50], the signs and magnitudes of thermodynamic parameters (ΔH (enthalpy change), and ΔS (entropy change)) for protein reactions can be used to identify the main forces contributing to protein stability. From the thermodynamics point of view, $\Delta H > 0$ and $\Delta S > 0$ suggest a hydrophobic interaction; $\Delta H < 0$ and $\Delta S < 0$ reflect van der Waals forces or hydrogen bonding; $\Delta H < 0$ and $\Delta S > 0$ suggest electrostatic forces play a key role. When there is no significant change in temperature, the enthalpy of the reaction can be considered as a constant in the formulas by which we calculated the thermodynamic parameters:

$$\ln K = -\frac{\Delta H}{RT} + \frac{\Delta S}{R} \quad (3)$$

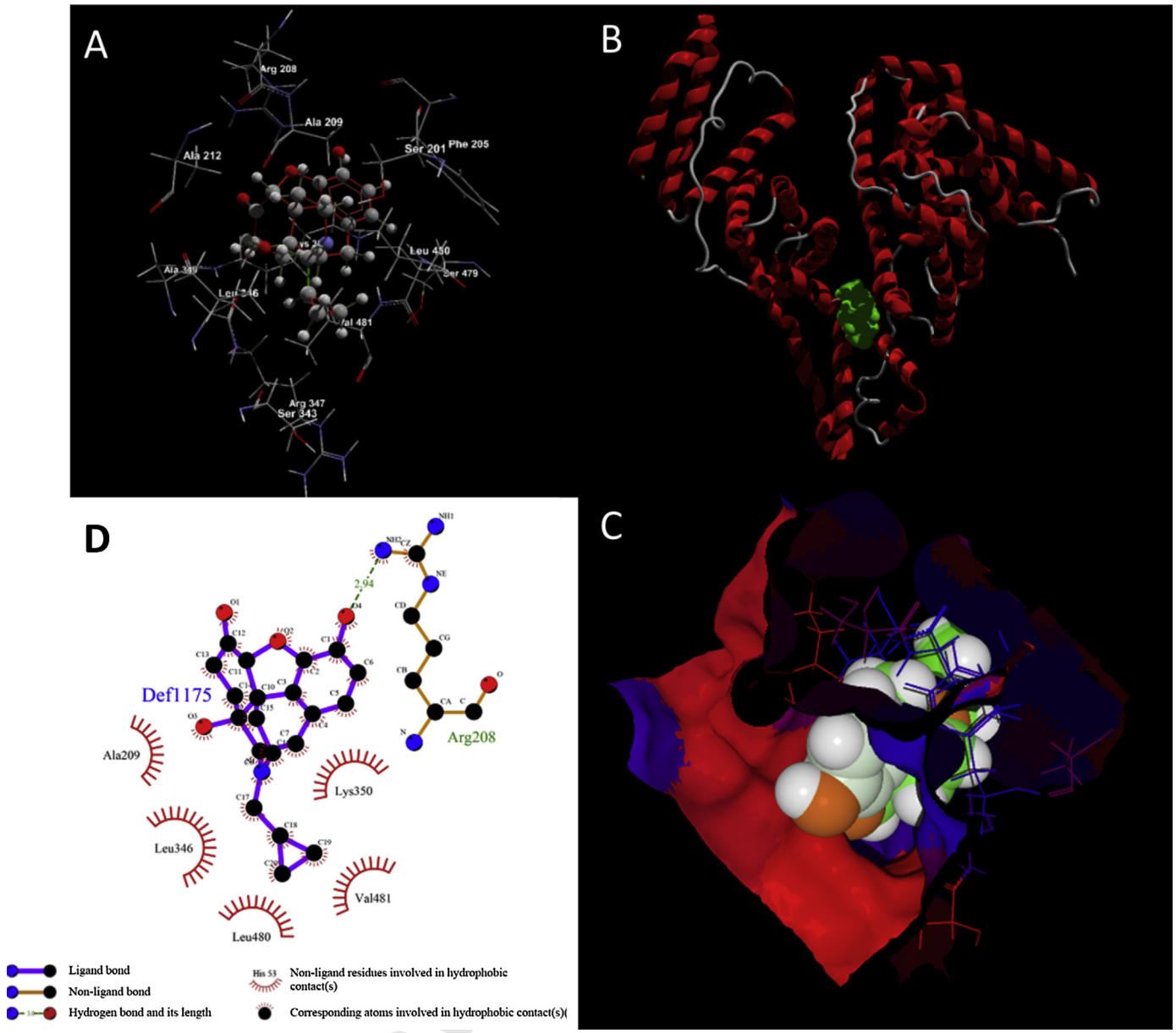

Fig. 4. Computer-generated models of NLT bound to BSA: (A) the residues of BSA are represented by sticks (thin) and the NLT is represented by ball and stick, (B) the NLT is shown as CPK and BSA is represented by solid ribbon, (C) the binding pocket of protein is represented by hydrophobic interaction and NLT is shown as CPK model, and (D) the output of LIGPLOT program.

where ΔG is free enthalpy change, R is the gas constant 8.314 J mol^{-1} K^{-1}, and T is the temperature. K represents the binding constant at the corresponding temperature. According to Eq. (3), the thermodynamic functions involved in the binding process were calculated and reported in Table 1. The negative sign for ΔG confirms that the binding process is spontaneous. The positive values of ΔS and ΔH revealed the predominance of hydrophobic interactions in the binding of FLR with BSA.

The same procedure (Fig. 5B) was used to study the interaction of NLT with BSA and the results are given in Table 1. The negative values of ΔS and ΔH reveal the predominance of Waals force or hydrogen bonding in the binding of NLT with BSA. With respect to

Table 1
Estimated thermodynamic parameters for BSA–FLR and BSA–NLT systems.

T (K)	10^{-4} K_a (M^{-1})	n	ΔH (KJ mol^{-1})	ΔS (J mol^{-1} K^{-1})	ΔG (KJ mol^{-1})
BSA–FLR					
298.15	4.9	0.93	38.7	175.4	−13.60
304.15	5.6	0.96			−14.65
310.15	6.1	1.01			−15.70
BSA–NLT					
298.15	28	1.92	−63.16	−153.2	−17.48
304.15	31	1.98			−16.56
310.15	33	2.03			−15.64

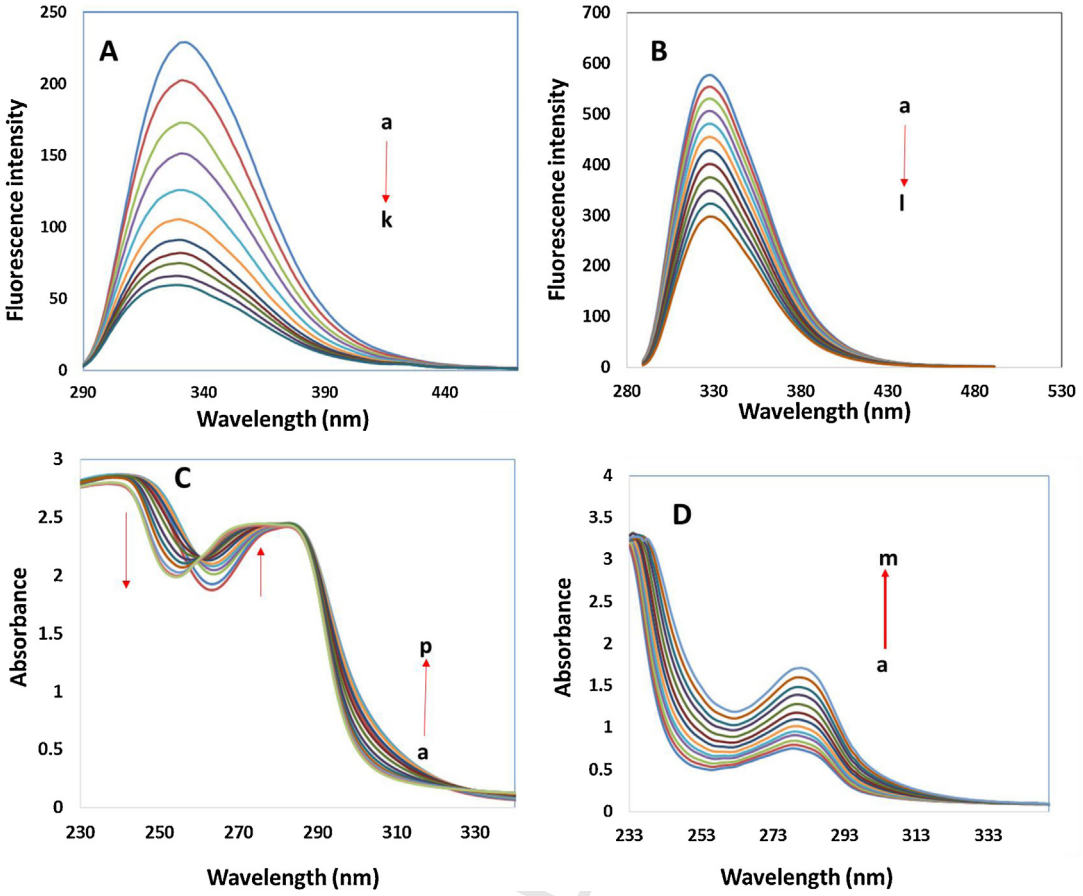

Fig. 5. (A) Fluorescence emission spectra of BSA–FLR system in TBS (0.05 M, pH 7.4) at 298.15 K: (a) free BSA (25.0 μM), and (b–k) BSA 25.0 μM with FLR at 5.0, 10.0, 20.0, 30.0, 40.0, 50.0, 60.0, 80.0, 90.0, and 100.0 μM, (B) Fluorescence emission spectra of BSA–NLT system in TBS (0.05 M, pH 7.4) at 298.15 K: (a) free BSA (50.0 μM), and (b–l) BSA 50.0 μM with NLT at 5.0, 10.0, 15.0, 25.0, 50.0, 75.0, 100.0, 125.0, 150.0, 175.0, and 200.0 μM, (C) UV–vis absorption spectra of NLT–BSA system in TBS (0.05 M, pH 7.4): (a) free NLT (5.0 μM), and (b–p) NLT 5.0 μM with BSA at 0.1, 0.25, 0.5, 0.75, 1.0, 1.25, 1.5, 1.75, 2.0, 2.5, 3.0, 3.5, 4.0, 4.5, and 5.0 μM, and (D) UV–vis absorption spectra of BSA–NLT system in TBS (0.05 M, pH 7.4): (a) free BSA (1.0 μM), and (b–m) BSA 1.0 μM with NLT at 0.05, 0.1, 0.25, 0.5, 0.75, 1.0, 1.5, 2.0, 2.5, 3.0, 3.5, and 4.0 μM.

the computational results it could be concluded that that the interaction of the NLT with BSA is mainly driven by hydrogen bonding.

3.2.1.2. UV–vis absorption studies. UV–vis absorption measurement is a simple but efficacious method to investigate structural changes and to confirm complex formation. Therefore, in order to investigate the structural changes in BSA and to confirm the complex formation between FLR and BSA, the UV–vis absorption measurements were made [51]. Upon addition of FLR to BSA hyperchromicity occurred in UV absorption spectra of BSA (not shown) which confirmed the absorption of FLR on BSA. The peak at 280.0 nm originates from the π–π^* transition of aromatic amino acid residues such as tryptophan and tyrosine [52]. The micro-environment surrounding amino acid residues are resolved by molecular conformation of the protein. Furthermore, the UV absorption spectra generate the corresponding change with alteration in micro-environment. Therefore, changes in the spectral characteristics of BSA can be used to judge conformational changes. The intensity of UV absorption spectra of BSA increased noticeably and a blue shift emerges in λ_{max} from 280 nm to 275 nm, conforming the increase in hydrophobicity of amino acid residues. Changes in λ_{max} indicated the change in peptide strand of BSA molecules and hence the change in hydrophobicity. According to these results, we concluded that the interaction between FLR and BSA led to changes in BSA conformation.

In order to investigate the structural changes in BSA upon binding to NLT and to confirm the complex formation between NLT and BSA, the interaction of NLT with BSA was monitored using UV–vis absorption measurements. The UV–vis absorption studies were carried out by keeping the NLT concentration constant and increasing the BSA concentration (Fig. 5C). It was evident that the intensity of UV absorption of NLT changed with the addition of BSA which are related to complex formation. The UV–vis absorption studies were also carried out by keeping the BSA concentration constant and increasing the NLT concentration (Fig. 5D). The absorption peak of BSA at 280.0 nm was found to be shifted to 6.0 nm toward higher wavelengths in the presence of increased amounts of NLT (Fig. 5D). According to these observations, we proposed that the binding between NLT and BSA led to changes in BSA conformation.

3.2.2. Morphological studies of the composite electrodes

A typical SEM image of the FLR/GCE clearly confirmed deposition of FLR at the surface of the GCE as shown in Fig. 6A. When BSA was immobilized onto the FLR/GCE surface the surface morphology was changed with slightly increasing the sizes of FLRs (Fig. 6B).

3.2.3. Optimization studies

In order to obtain suitable assay results, the effects of some parameters have been investigated in detail. It was found that the amounts of FLR and BSA deposited on the biosensor surface, and incubation time with NLT greatly affected the EIS response of the proposed biosensor. For optimizing the recorded EIS signal, the performance of the biosensors fabricated with different concentrations of FLR (0.1, 0.2, 0.3, 0.4, 0.5, 0.6 and 0.65 mg mL^{-1}) and BSA (0.5, 0.45,

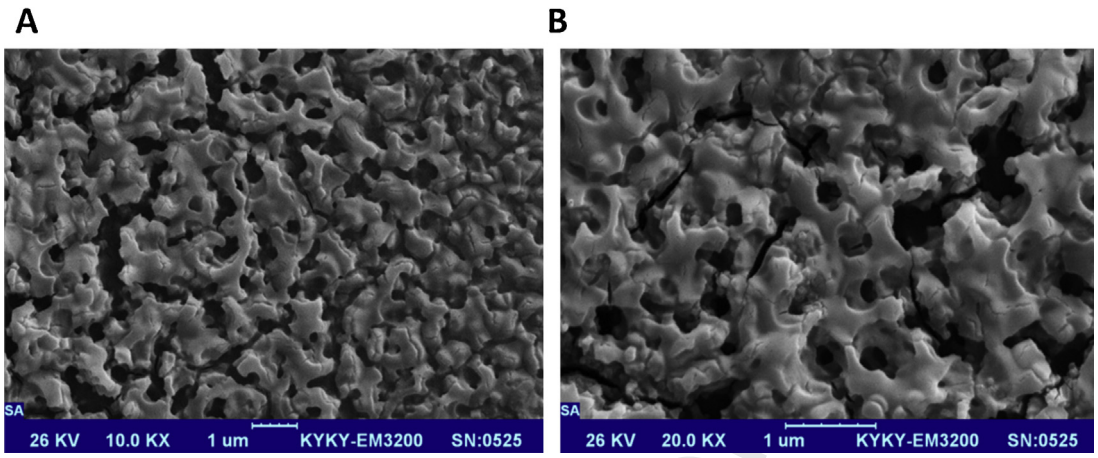

Fig. 6. SEM images of (A) FLR/GCE, and (B) BSA/FLR/GCE.

0.4, 0.35, 0.3, 0.25, and 0.2 mg mL^{-1}) was studied under different incubation times (45, 40, 35, 30, 25, 20, and 15 min) with the same concentration of 10.0 nM NLT. The changes in R_{ct} (charge transfer resistance) were used to characterize the changes in biosensor surface. The results clearly confirmed that the R_{ct} decreased with the increase of amount of FLR when the concentration of FLR was 0.65 mg mL^{-1} (Fig. 7A). Therefore, 0.65 mg mL^{-1} FLR was chosen as the optimized concentration of Gr for the next measurements. Then, effects of amount of BSA on FLR/GCE surface and incubation time of BSA/FLR/GCE with NLT were investigated. It was observed that the R_{ct} decreased with the decrease of both amount of BSA (Fig. 7B) and incubation time (Fig. 7C), when the concentration of BSA and incubation time were 0.2 mg mL^{-1}and 15.0 min, respectively. Therefore, these optimized values were used for the next measurements.

3.2.4. Electrochemical studies

The CVs of 5.0 mM $[Fe(CN)_6]^{3-/4-}$ in TBS 0.05 M, pH 7.4 at a scan rate of 50.0 mV s^{-1} on bare GCE, FLR/GCE, BSA/FLR/GCE, and also BSA/FLR/GCE incubated with NLT (10.0 nM) for 15.0 min were recorded and are shown in Fig. 8A. A standard redox peak could be observed for the bare GCE (Fig. 8A, curve a). The background currents and the redox peaks' currents of FLR/GCE, and BSA/FLR/GCE (Fig. 8A, curves b and c) are larger than those of bare GCE, which confirmed that they have larger effective surface areas. After modification of the bare GCE with FLR, the peak currents and ΔE_P increased and decreased, respectively, which confirmed the enhancement in the electron transfer rate at the FLR/GCE surface. After modification of the FLR/GCE with BSA, it could be seen that the redox currents of the probe decreased, the peak potentials change a little, and no new peak was observed in the same potential scanning range. Therefore, it can be concluded that the presence of BSA inhibits the interfacial electron transfer in some extent due to the non-conductive properties of BSA. When the BSA/FLR/GCE was further incubated in NLT solution (10.0 nM) for 15.0 min, it could be seen that the redox currents and the ΔE_P decreased and increased, respectively (Fig. 8A, curve d). Therefore, according to these observations and the new peak at 0.493 V, it was proposed that the NLT may form a negatively charged electroactive complex with BSA which decelerates the electron transfer of the negatively charged redox probe due to the electrostatic repulsion between the biosensor surface and the redox couple ions carrying negative charge.

Change in peak current may be related to the change in the effective surface area of the electrode. Therefore, to investigate this parameter, the surface areas of the prepared electrodes were investigated by the Randles-Sevcik equation (298.15 K), using the redox currents of the redox probe (i_p):

$$i_p = (2.687 \times 10^5) n^{3/2} \upsilon^{1/2} D^{1/2} AC \quad (4)$$

where D, the diffusion coefficient of the ferricyanide, was 6.3×10^{-6} cm^2 s^{-1}; n and C represent the transferring electron number and the concentration (mol dm^{-3}) of the ferricyanide; υ was the scan rate (V s^{-1}); and A was the surface area (cm^2).

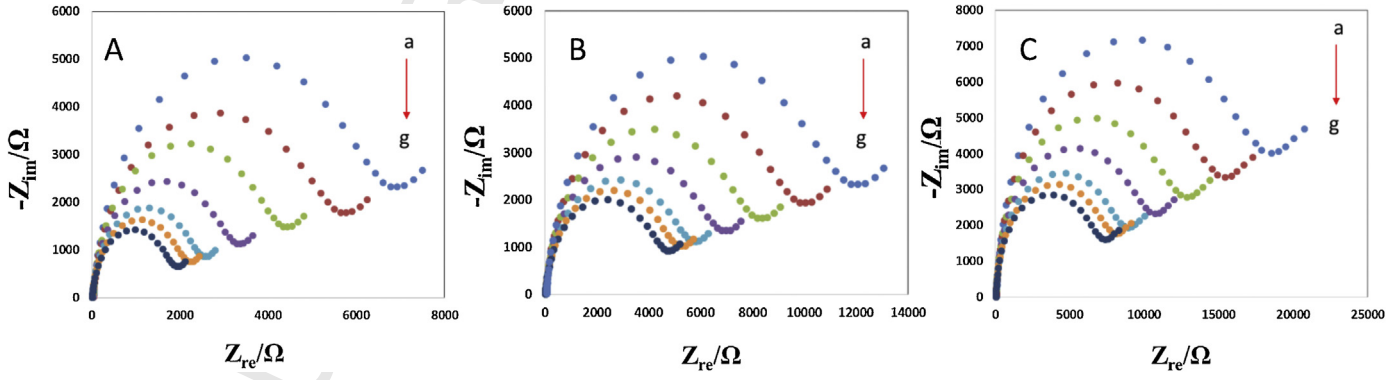

Fig. 7. Optimization procedures in 5.0 mM $[Fe(CN)_6]^{4-/3}$ in TBS (0.05 M, pH 7.4): (A) effects of FLR concentration on EIS response of the propsed biosensor (conditions: BSA:0.2 mg mL^{-1}, NLT: 10.0 nM, incubation time: 15 min, and FLR: 0.1, 0.2, 0.3, 0.4, 0.5, 0.6 and 0.65 mg mL^{-1} (curves a–g)), (B) effects of BSA concentration on EIS response of the propsed biosensor (conditions: FLR: 0.65 mg mL^{-1}, NLT: 10.0 nM, incubation time: 15 min, and BSA: 0.5, 0.45, 0.4, 0.35, 0.3, 0.25, and 0.2 mg mL^{-1} (curves a–g)), and (C) effects of incubation time on EIS response of the propsed biosensor (conditions: FLR: 0.65 mg mL^{-1}, BSA: 0.2 mg mL^{-1}, NLT: 10.0 nM, and incubation time: 45, 40, 35, 30, 25, 20, and 15 min (curves a–g)).

Please cite this article in press as: M.-B. Gholivand, et al., Int. J. Biol. Macromol. (2014), http://dx.doi.org/10.1016/j.ijbiomac.2014.07.028

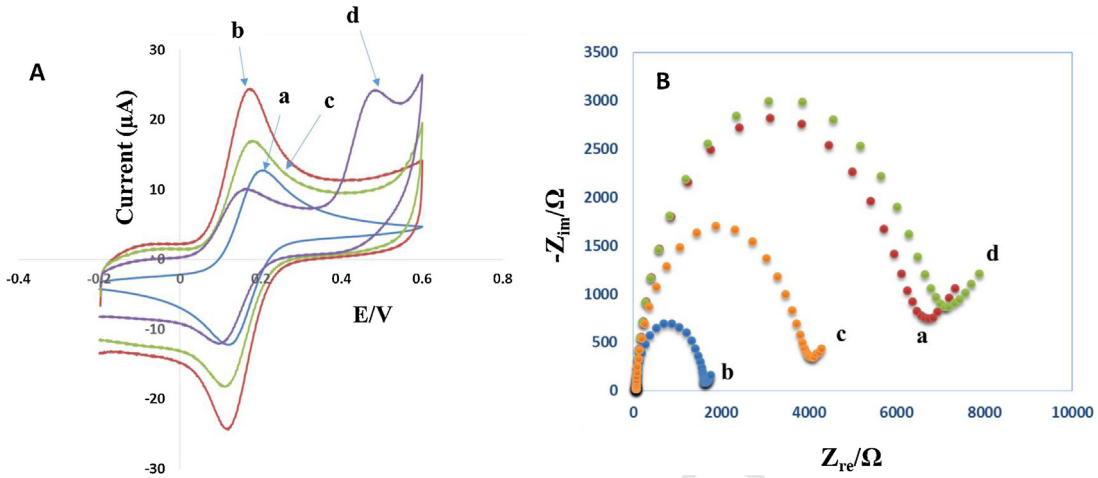

Fig. 8. (A) CVs and (B) EISs of 5.0 mM $[Fe(CN)_6]^{4-/3}$ in TBS 0.05 M, pH 7.4 at a scan rate of 50 mV s^{-1} on (a) bare GCE, (b) FLR/GCE, (c) BSA/FLR/GCE, and (d) BSA/FLR/GCE incubated with NLT (10.0 nM) for 15 min.

The surface areas of the bare GCE, FLR/GCE, BSA/FLR/GCE, and BSA/FLR/GCE incubated with NLT (10.0 nM) for 15.0 min were calculated to be 0.12, 0.45, 0.22, and 0.14 cm^2, respectively.

The EIS can be considered as an effective method for probing the features of interfacial electron-transfer resistance during the modification process. In the Nyquist diagram, the diameter of the semicircle reflects the R_{ct} of redox conversion of $[Fe(CN)_6]^{3-/4-}$ on the electrode surface. In this study, we investigated the changes in R_{ct} during the modification process. The electron transfer process is caused by the presence of the redox couple in the bulk solution and any modification of the electrode surface strongly influences its electrochemical nature, which leads to a change in the R_{ct} value. Fig. 8B, shows the EISs of bare GCE (curve a), FLR/GCE (curve b), BSA/FLR/GCE (curve c), and BSA/FLR/GCE after treatment with NLT (10.0 nM) for 15.0 min (curve d) in the presence of 5.0 mM $[Fe(CN)_6]^{3-/4-}$ in TBS 0.05 M, pH 7.4. As can be seen a semicircle with R_{ct} about 6.7 kΩ was obtained at the bare GCE. However, the diameter of the semicircle was changed to 1.7 kΩ and 4.03 kΩ by modification of the bare GCE with FLR, and BSA/FLR, respectively, which suggested acceleration and deceleration for $[Fe(CN)_6]^{3-/4-}$ redox reaction due to the presence of FLR and BSA, respectively. A reason for the increase in the R_{ct} value during the modification of FLR/GCE with BSA is that BSA acts as an inert electron layer which hinders the interfacial electron transfer in some extent. In the other hand, by treating the BSA/FLR/GCE with NLT, the interfacial electron resistance increased (7.18 kΩ) coinciding with the CV results. Therefore, the presence of NLT may result in the deactivation of the BSA/FLR/GCE surface by forming a negatively charged electroactive complex with BSA which repels the negatively charged redox probe and decelerates the interfacial electron transfer which leads to obvious faradaic impedance change.

3.2.5. Analytical applications

3.2.5.1. NLT determination. Under the optimized condition, the relationship between R_{ct} values and the NLT concentrations was investigated using EIS and the results are shown in Fig. 9. According to the in inset of Fig. 9, there is a linear relationship between R_{ct} and NLT concentration over a concentration range from 0.1 nM to 80.0 nM (R^2 0.9927). The linear response obtained by the proposed biosensor in this work indicated that the biosensor could be possibly used in the analysis of real samples. The limit of detection (LOD) of this method was calculated ($3S_b/b$, where S_b is the standard deviation ($n = 6$) of the blanks, and b is the slope of the calibration graph) to be 0.01 nM. Comparing with the results reported by some works [32,33,53], this value is superior to available reports. Furthermore, the sensitivity of the proposed method was calculated to be

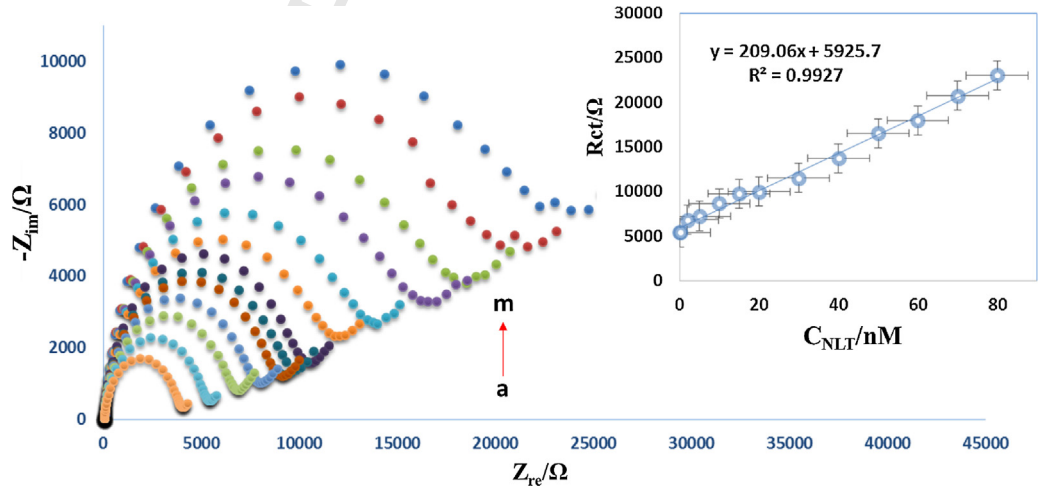

Fig. 9. (A) EIS curves of the BSA/FLR/GCE in 5.0 mM $[Fe(CN)_6]^{3-/4-}$ in TBS 0.05 M, pH 7.4 corresponding to different concentrations of NLT: (a) 0, (b) 0.1 nM, (c) 2 nM, (d) 5 nM, (e) 10 nM, (f) 15 nM, (g) 20 nM, (h) 30 nM, (i) 40 nM, (j) 50 nM, (k) 60 nM, (l) 70 nM, and (m) 80 nM. Inset: The corresponding calibration plot of R_{ct} versus different concentrations of NLT.

Table 2
Determination of NLT in urine samples ($n = 3$).

Samples	Added (nM)	Found (nM)	Recovery (%)	HPLC-UV
Urine[a]	10.0	9.9 ± 0.1	99.0	10.0 ± 0.1
	5.0	5.1 ± 0.1	102.0	5.0 ± 0.1
	–	<LOD	–	<LOD
	3.0	3.1 ± 0.1	103.2	3.0 ± 0.1
Urine[b]	–	4.2 ± 0.1	–	−4.0 ± 0.1
	2.0	6.1 ± 0.1	104.8	6.0 ± 0.1
	15.0	18.9 ± 0.3	99.4	18.1 ± 0.2
	20.0	24.6 ± 0.4	102.9	24.1 ± 0.1

[a] Healthy.
[b] Addict.

0.2 kΩ nM^{-1} from the slope of the calibration graph, indicating the high sensitivity of the proposed sensing system.

3.2.5.2. Stability, repeatability, and reproducibility. The stability of BSA/FLR/GCE was investigated by measuring a solution of 10.0 nM NLT in 5.0 mM $[Fe(CN)_6]^{3-/4-}$ in TBS (0.05 M, pH 7.4). After ten days, the proposed biosensor retained 93.1% of its initial response. After one month, the biosensor response decreased about 9.5%. It was observed that the stability of the proposed biosensor was affected by the time of immersing the biosensor in the cell solution. Therefore, the effect of this parameter on the biosensor stability was investigated and it was found that the biosensor did not show good stability when it continued in contact with the cell solution for more than 5.0 h. Therefore, it is recommended to remove the biosensor from cell solution during the breaks between measurements. The repeatability of the proposed biosensor was investigated for ten times within the same day giving satisfied relative standard deviation (RSD) of 4.3%. The reproducibility of the BSA/FLR/GCE was examined by recording the EIS responses of six individual biosensors in 5.0 mM $[Fe(CN)_6]^{3-/4-}$ in TBS (0.05 M, pH 7.4) containing 10.0 nM NLT and the *RSD* was got as 5.1%. The above results indicated the good stability, repeatability, and reproducibility of the proposed biosensor.

3.2.5.3. Interference study. To evaluate the selectivity of the proposed biosensor, some possible interfering species such as thiourea, dopamine, uric acid, urea, sorbitol, citric acid, sucrose, fructose, glucose, epinephrine, norepinephrine, ascorbic acid, histidine, valine, glycine, tyrosine, tryptophan and alanine which may be present in real samples, were tested in TBS (0.05 M, pH 7.4), in the presence of NLT (10.0 nM). After the experiment, we concluded that, 50.0-fold thiourea, dopamine, uric acid, urea, sorbitol, and citric acid, 150.0-fold sucrose, fructose, epinephrine, and norepinephrine, 100.0-fold glucose, and ascorbic acid, and 120.0-fold histidine, valine, glycine, tyrosine, tryptophan and alanine did not show remarkable interference to NLT detection.

3.2.5.4. Determination of NLT in real samples. To examine the BSA/FLR/GCE's ability to determination of NLT, we tested its ability to detect NLT in urine samples of both healthy and addict volunteers. Results are shown in Table 2. As can be seen, good recoveries were obtained which suggested that the proposed biosensor was both effective and sensitive for determination of NLT in real samples. The accuracy of the proposed method in this study was also compared with the HPLC results. The results presented in Table 2 confirm that the proposed biosensor shows a good accuracy for determination of NLT in real samples. Therefore, the successful detection of NLT in biological samples as demonstrated here may be straightforward when testing for NLT clinically.

4. Conclusions

In conclusion, a computationally engineered nanobiocomposite based on immobilization of BSA onto FLR was used to construct an ultrasensitive impedimetric NLT biosensor. The computational results were confirmed by experimental observations. The proposed biosensor exhibited stable, regenerable, and sensitive functions for NLT determination. The characterizations performed by CV, and EIS suggest that the incubation of BSA/FLR/GCE with NLT significantly decreases the electrode surface area which leads to obvious faradaic impedance changes. The present work not only provides a better understanding of parameters involved in the development of BSA/FLR nanobiocomposite, but also shows the advantages related to the use of computational techniques in developing new and efficient biosensors. The principles used in this study could potentially be used to construct new biosensors in clinical settings for biological fluids.

Acknowledgements

The authors gratefully acknowledge the financial supports of this project by the Razi University Research Council, UNL, CONICET and ANPCyT. The authors would like to thank the reviewers for their insightful comments which led to an improvement of the work.

References

[1] R.I. Shader, J. Clin. Psychopharmacol. 23 (2003) 321.
[2] M.E. Wall, D.R. Brine, M. Perez-Reyes, Drug Metab. Dispos. 9 (1981) 369.
[3] K. Verebey, M.J. Kogan, A. DePace, J.M. Salvatore, J. Chromatogr. A 118 (1976) 331.
[4] R.H. Reuning, S.B. Ashcraft, B.E. Morrison, NIDA Res. Monogr. Ser. 28 (1981) 33.
[5] K. Verebey, D. De Pace, D. Jukofsky, J. Volavka, S.J. Mule, J. Anal. Toxicol. 4 (1980) 33.
[6] G.L. Burce, H.B. Bhat, T. Sokoloski, J. Chromatogr. 137 (1977) 323.
[7] R.H. Reuning, V.K. Batra, T.M. Ludden, M.Y. Jao, B.E. Morrison, D.A. McCarthy, S.E. Harrigan, S.B. Ashcraft, R.A. Sams, M.S. Bathala, A.E. Staubus, L. Malspeis, J. Pharm. Sci. 68 (1979) 411.
[8] R.A. Sams, L. Malspeis, J. Chromatogr. 125 (1976) 409.
[9] C.C. Nelson, M.D. Fraser, J.K. Wilfahrt, R.L. Foltz, Ther. Drug Monit. 15 (1993) 557.
[10] W. Huang, D.E. Moody, R.L. Foltz, S.L. Walsh, J. Anal. Toxicol. 21 (1997) 252.
[11] K.M. Monti, R.L. Foltz, D.M. Chinn, J. Anal. Toxicol. 15 (1991) 136.
[12] C.F. Chan, G.M. Chiswell, R. Bencini, L.P. Hackett, L.J. Dusci, K.F. Ilett, J. Chromatogr. B 761 (2001) 85.
[13] S.W. Toennes, G.F. Kauert, S.M. Grusser, W. Jakel, G. Partecke, J. Pharm. Biomed. Anal. 35 (2004) 169.
[14] A.F. Davidson, T.A. Emm, J. Pieniaszek, J. Pharm. Biomed. Anal. 14 (1996) 1717.
[15] H. Derendorf, A.E. El Koussi, E.R. Garrett, J. Pharm. Sci. 73 (1984) 621.
[16] W.J. Hurst, I.S. Zagon, H.Y. Boul-Enein, Pharmazie 54 (1999) 595.
[17] K. Kambia, S. Bah, T. Dine, R. Azar, P. Odou, B. Gressier, M. Luyckx, C. Brunet, L. Ballester, M. Cazin, J.C. Cazin, Biomed. Chromatogr. 14 (2000) 151.
[18] C. Kim, R. Cheng, W.A. Corrigall, Chromatographia 25 (1988) 91.
[19] M.C. Meyer, A.B. Straughn, M.W. Lo, W.L. Schary, C.C. Whitney, Clin. Psychiatry 45 (1984) 15.
[20] E.F. O'Connor, S.W.T. Cheng, W.G. North, J. Chromatogr. B: Biomed. Appl. 491 (1989) 240.
[21] K.K. Peh, N. Billa, K.H. Yuen, J. Chromatogr. B: Biomed. Appl. 701 (1997) 140.
[22] K. Sarkka, K. Ariniemi, P. Lillsunde, Z Zagadnien Nauk Sadowych 43 (2000) 250.
[23] P. Zuccaro, I. Altieri, P. Bette, R. Pacifici, G. Ricciarello, L.A. Pini, E. Sternieri, S. Pichini, J. Chromatogr. B: Biomed. Appl. 576 (1991) 485.
[24] L. Olsen, A.S. Christopherson, G. Fropsahl, H. Waal, J. Morland, Br. J. Clin. Pharmacol. 58 (2004) 219.
[25] S. Valiveti, B.N. Nalluri, D.C. Hammell, K.S. Paudel, A.L. Stinchcomb, J. Chromatogr. B 810 (2004) 259.
[26] S.S. Iyer, G.E. Kellogg, H.T. Karnes, J. Chromatogr. Sci. 45 (2007) 694.
[27] M.H. Slawson, M. Chen, D.E. Moody, S.D. Comer, E.S. Nuwayser, W.B. Fang, R.L. Foltz, J. Anal. Toxicol. 31 (2007) 453.
[28] A. Campiglio, Analyst 123 (1998) 1053.
[29] Z.R. Fernandez-Abedul, A. Costa-Garcia, J. Pharm. Biomed. Anal. 16 (1997) 15.
[30] P. Murillo, L.F. Bermejo, J.L. Garrido, J.L. Lara, Anal. Chim. Acta 495 (2003) 249.
[31] Z.R. Fernandez-Abedu, R. Barreira, G. Costa, Anal. Lett. 30 (1997) 1491.
[32] M.M. Ghoneim, H.S. El-Desoky, M.M. Abdel-Galeil, Bioelectrochemistry 81 (2011) 65.
[33] F. Ghorbani-Bidkorbeh, S. Shahrokhian, A. Mohammadi, R. Dinarvand, J. Electroanal. Chem. 638 (2010) 212.

[34] H.W. Kroto, J.R. Heath, S.C. O'Brien, R.F. Curl, R.E. Smalley, Nature 318 (1985) 162.
[35] S. Griese, D.K. Kampouris, R.O. Kadara, C.E. Banks, Electroanalysis 20 (2008) 1507.
[36] E. Nakamura, H. Isobe, Acc. Chem. Res. 36 (2003) 807.
[37] C.A. Martin, D. Ding, J.K. Sørensen, T. Bjørnholm, J.M. van Ruitenbeek, H.S.J. van der Zant, J. Am. Chem. Soc. 130 (2008) 13198.
[38] J.T. Robinson, F.K. Perkins, E.S. Snow, Z. Wei, P.E. Sheehan, Nano Lett. 8 (2008) 3137.
[39] B.C. Thompson, J.M.J. Frechet, Angew. Chem. Int. Ed. 47 (2008) 58.
[40] Y.F.E.L.L. Bai, L.Z. Fan, M. Han, X.Y. Zhang, S.H. Yang, J. Mater. Chem. 21 (2011) 819.
[41] E. Grodzka, P. Pieta, P. Dluzewski, W. Kutner, K. Winkler, Electrochim. Acta 54 (2009) 5621.
[42] M. Csiszar, A. Szucs, M. Tolgyesi, A. Mechler, J.B. Nagy, M.J. Novak, J. Electroanal. Chem. 497 (2001) 69.
[43] R.N. Goyal, V.K. Gupta, N. Bachheti, R.A. Sharma, Electroanalysis 20 (2008) 757.
[44] N. Sun, L. Guan, Z. Shi, Z. Zhu, N. Li, M. Li, Z. Gu, Electrochem. Commun. 7 (2005) 1148.
[45] A.C. Wallace, R.A. Laskowski, J.M. Thornton, Protein Eng. 8 (1995) 127.
[46] M. Csiszar, A. Szucs, M. Tolgyesi, A. Mechler, J.B. Nagy, M. Novak, J. Electroanal. Chem. 497 (2001) 69.
[47] J.H. Suh, Y.Y. Lee, H.J. Lee, M. Kang, Y. Hur, S.N. Lee, D.H. Yang, S.B. Han, J. Pharm. Biomed. Anal. 75 (2013) 214.
[48] J.R. Lakowicz, Principles of Fluorescence Spectroscopy, 3rd ed., Springer Press, New York, 2006.
[49] Y.J. Hu, Y. Liu, X.H. Xiao, Biomacromolecules 10 (2009) 517.
[50] P.D. Ross, S. Subramanian, Biochemistry 20 (1981) 3096.
[51] S. Bi, D. Song, Y. Tian, X. Zhou, Z. Liu, H. Zhang, Spectrochim. Acta Part A 61 (2005) 629.
[52] A.N. Glazer, E. Smitth, J. Biochem. 236 (1961) 2942.
[53] S. Shahrokhian, Z. Kamalzadeh, R. Saberi, Electroanalysis 23 (2011) 2925.

Please cite this article in press as: M.-B. Gholivand, et al., Int. J. Biol. Macromol. (2014), http://dx.doi.org/10.1016/j.ijbiomac.2014.07.028